

Effects of rates of spontaneous synaptic vesicle secretions in inner hair cells on information transmission in an auditory nerve fiber model

Parichat Kumsa, *Student Member IEEE*, and Hiroyuki Mino, *Senior Member IEEE*

Abstract—In this article, we investigate how the rates of spontaneous synaptic vesicle secretions affect information transmission of the spike trains in response to the inner hair cell (IHC) synaptic currents in an auditory nerve fiber (ANF) model through computer simulations. The IHC synaptic currents were modeled by a filtered inhomogeneous Poisson process modulated with sinusoidal functions, while the stochastic ion channel model was incorporated into each node of Ranvier in the ANF model with spiral ganglion. The information rates were estimated from the entropies of the inter-spike intervals of the spike trains to evaluate information transmission in the ANF model. The results show that the information rates increased, reached a maximum, and then decreased as the rate of spontaneous secretion increased, implying a resonance phenomenon dependent on the rate of spontaneous IHC synaptic secretions. In conclusion, this phenomenon similar to the regular stochastic resonance may be observed due to that spontaneous IHC synaptic secretions may act as an origin of fluctuation or noise, and these findings may play a key role in the design of better auditory prostheses.

Index Terms—Stochastic Resonance, Inner Hair Cell Synapse, Inhomogeneous Poisson process, Auditory Nerve Fiber Model, Stochastic Hodgkin-Huxley Model, Neural Spike Trains

I. INTRODUCTION

Spontaneous spikes refer to the action potentials fired even without any stimulus in nervous systems. These are specified quantitatively by the rate of spikes, the count of action potentials per unit time in which the time intervals between them are characterized approximately by the exponential probability density function with a dead time (absolute refractory period) [1]. In inner hair cells (IHCs) of the organ of Corti, spontaneous synaptic vesicle secretions are considered trigger spontaneous spikes in postsynaptic neurons, i.e., auditory nerve fibers (ANFs), in a manner of the one-to-one correspondense between synaptic vesicle secretions and spikes.

The spontaneous spikes are supposed to be detrimental to information transmission of spike trains in nervous systems, since they do not carry any information on stimuli. On the other hand, it has been reported in [2], [3], [4], [5] that several tens of spontaneous spikes were observed in an auditory nerve fiber of cats, suggesting that they would play a key role in relaying sounds into cochlear nucleus in the brainstem. However, it has been unclear how the spontaneous spikes generated by the IHC synaptic vesicles can affect

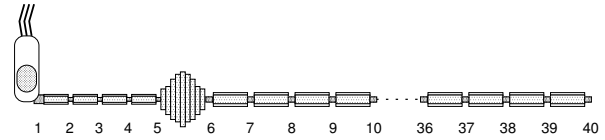


Fig. 1. Auditory nerve fiber model : there is a spiral ganglion on the center. There is an inner hair cell with synapse on the axon tip of the peripheral side, while the axon of the central side is assumed to be connected to cochlear nucleus in brain stem. This ANF model possesses 40 nodes of Ranvier. The IHC synaptic current was applied into the 1-st node of Ranvier, while the transmembrane potentials were recorded at the 36-th node of Ranvier to generate the spike trains. Note that this figure is not scaled in length.

information transmission of the spike trains in auditory nerves, although a pseudo-spontaneous activity was investigated in cochlear implant stimulation [6].

The objective of this research was to investigate, through computer simulations, how the rates of spontaneous synaptic vesicle secretions generating the spontaneous spikes would affect information transmission of the spike trains in response to the IHC synaptic currents in an ANF model.

II. METHODS

The auditory nerve fiber model with the spiral ganglion was composed of 40 sections of the node and myelin, represented by the multi compartment model as shown in Figure 1(a) [7], [8]. We note that the scale of this figure is not correct. The diameter of the myelin of the peripheral side was set at $2.0 \mu\text{m}$, the length of the long axis of the myelin part was $184 \mu\text{m}$, the diameter of the node of Ranvier was set at $1.2 \mu\text{m}$ and the width of the gap of node was $1.0 \mu\text{m}$. On the other hand, the diameter of the myelin of the central side was set at $2.5 \mu\text{m}$, the length of the long axis of the myelin was $230 \mu\text{m}$, the diameter of the node of Ranvier was $1.5 \mu\text{m}$ and the width of the gap of node was set at $1.0 \mu\text{m}$. Figure 2(a) shows the corresponding electric equivalent circuit of the myelinated nerve fiber of the central side. In this model, the stochastic ion channel models were incorporated into each node of Ranvier, as shown in Figure 2(b), in which the switch expresses the open and closed states of the two states ion channel gatings of Na and K channels according to a discrete-state Markov process [9]. The other parameters were adopted from those in [7], [8].

The membrane potentials as functions of time t and space k can be expressed as a set of partial difference equations of the diffusion type. In practical situations, the continuous system was solved numerically by digital computers using

P. Kumsa is with Graduate School of Engineering, Kanto Gakuin University, 1-50-1 Mitsuura E., Kanazawa-ku, Yokohama 236-8501, Japan paramod_chat@hotmail.com, H. Mino is with Department of Electrical and Computer Engineering, Kanto Gakuin University, 1-50-1 Mitsuura E., Kanazawa-ku, Yokohama 236-8501, Japan mino@ieee.org

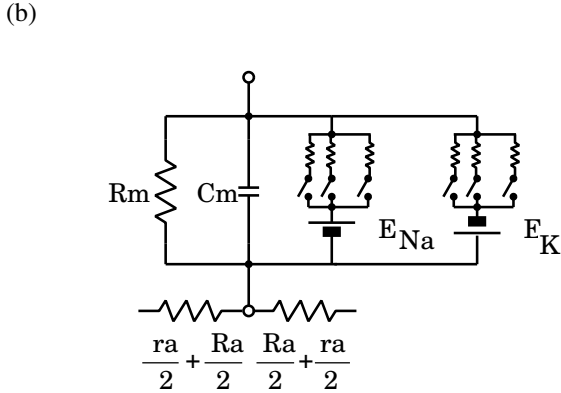
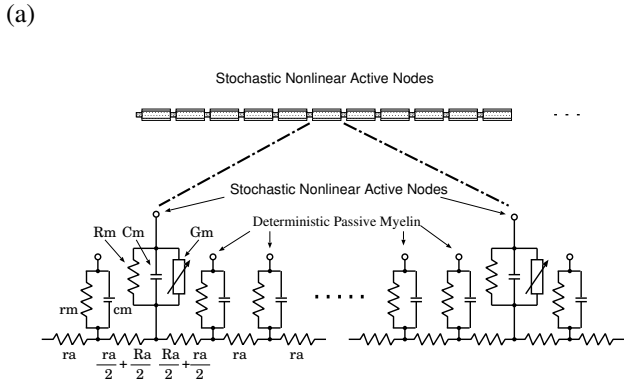


Fig. 2. (a) Electric equivalent circuit of the axon in the central side of the ANF model (b) Electric equivalent circuit of each node of Ranvier where stochastic ion channels were incorporated (Na :130 channel,22.65 ρ S,K :50 channel,50.0 ρ S)

the following equations [7] :

$$\left(\frac{V_m^{[k+1]}[t] - V_m^{[k]}[t]}{R_a^{[k+1,k]}} - \frac{V_m^{[k]}[t] - V_m^{[k-1]}[t]}{R_a^{[k,k-1]}} \right) = C_m^{[k]} \frac{V_m^{[k]}[t + \Delta t] - V_m^{[k]}[t]}{\Delta t} + \frac{V_m^{[k]}[t]}{R_m^{[k]}} + I_{ion}^{[k]}[t]$$

where

$$I_{ion}^{[k]}[t] = \begin{cases} \gamma_{Na} N_{Na}^{[k]}[t] (V_m^{[k]}[t] - E_{Na}) + \gamma_K N_K^{[k]}[t] - E_K & (atnode) \\ 0 & (otherwise) \end{cases} \quad (1)$$

where $N_{Na}^{[k]}[t]$ and $N_K^{[k]}[t]$, the number of open channels in Na and K channel, are expressed as functions of time t and space k . In computer simulations, the membrane potentials $V_m^{[k]}[t]$ can be solved numerically with by the Crank-Nicholson method.

The IHC synaptic current was applied to the first node of Ranvier of the peripheral side, and was modeled by a filtered inhomogeneous Poisson process[1] expressed as :

$$I_{ihc}(t) = \int_{-\infty}^t i_{ihc}(t - \tau) dN_{ihc}(\tau) \quad (2)$$

$$i_{ihc}(t) = \begin{cases} I_{amp} & (0 \leq t \leq \tau_{max}) \\ 0 & (otherwise) \end{cases} \quad (3)$$

where $I_{amp}=6 \text{ nA}$, $\tau_{max}=1 \text{ ms}$, and $N_{ihc}(t)$ denotes the counting process of the inhomogeneous Poisson process[1], characterized by the intensity function :

$$\lambda_{ihc}(t) = \lambda_{spon} + \tilde{\lambda}_{sinusoid}(t) \quad (4)$$

$$\tilde{\lambda}_{sinusoid}(t) = \begin{cases} \lambda_c \cos(2\pi ft) & (\tilde{\lambda}_{sinusoid}(t) > 0) \\ 0 & (otherwise) \end{cases} \quad (5)$$

where $f=440 \text{ Hz}$, $\lambda_c=200 \text{ s}^{-1}$. In computer simulations, λ_{spon} was set at 10, 20, 30, 40, 60, 80, and 100 s^{-1} to investigate its dependency on information transmission.

An illustrative example is shown in which the transmembrane potentials at the 36-th node of Ranvier (top), the IHC synaptic current (middle), and the intensity function of inhomogeneous Poisson process at $\lambda_{spon}=40 \text{ s}^{-1}$, $f=440 \text{ Hz}$, and $\lambda_c=200 \text{ s}^{-1}$, as depicted in Figure 3.

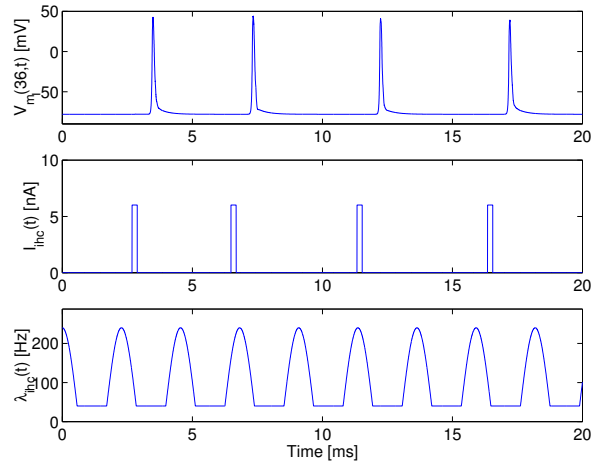


Fig. 3. The transmembrane potentials at the 36-th node of Ranvier (top), the IHC synaptic current (middle), and the intensity function of inhomogeneous Poisson process at $\lambda_{spon}=40 \text{ s}^{-1}$, $f=440 \text{ Hz}$, and $\lambda_c=200 \text{ s}^{-1}$

The information rates of the spike trains recorded at the 36th node of Ranvier was estimated by calculating the total and noise entropies, from the inter-spike interval of spike firing times, T , as follows [10] :

$$I_{rate}(T, I_{ihc}(t)) = R[H(T) - H(T|I_{ihc}(t))] \quad (6)$$

where

$$H(T) = - \sum_{i=0}^{\infty} p(T_i) \log_2 P(T_i)$$

$$H(T|I_{ihc}) = -E \left[\sum_{i=0}^{\infty} p(T_i|I_{ihc}(t)) \log_2 P(T_i|I_{ihc}(t)) \right]$$

in which $H(T)$ and $H(T|I_{ihc}(t))$ denote the total entropy of inter spike intervals (ISIs), and the noise entropy of ISIs, given the condition on the inner hair cell synaptic current, $I_{ihc}(t)$. R stands for spike rates, and $E[\]$ designates the expectation operation.

III. RESULTS

In computer simulations, the rate of spontaneous IHC synaptic vesicle secretions, λ_{spon} , was varied to see how λ_{spon} would affect the properties of encoding the sinusoidal functions into the spike trains and the information transmission.

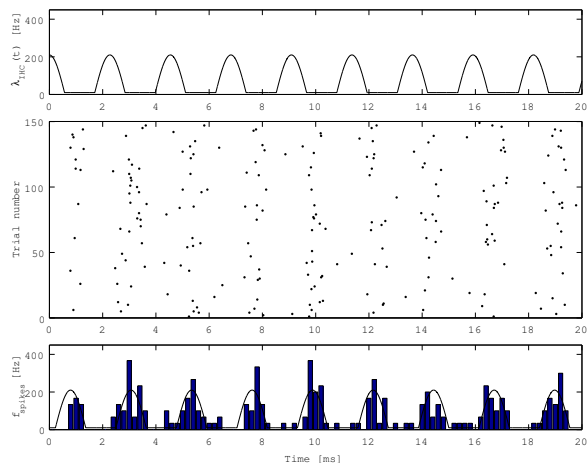


Fig. 4. Intensity function (top trace), Raster plot (middle trace), Post-stimulus time histogram with an intensity function (bottom trace) at $\lambda_{spon} = 10s^{-1}$, $\lambda_c=200 s^{-1}$, and $f = 440Hz$

Figure 4 depicts the intensity function(top trace), raster plot(middle trace), post-stimulus time histogram (PSTH) with an intensity function(bottom trace) at $\lambda_{spon} = 10s^{-1}$, $\lambda_c=200 s^{-1}$, and $f = 440Hz$. In this figure, the raster plot seems to synchronize to a frequency of $440 Hz$, however, it was observed that the sinusoids were not necessarily encoded well into the spike trains, because the PSTH was not agreed with the intensity function.

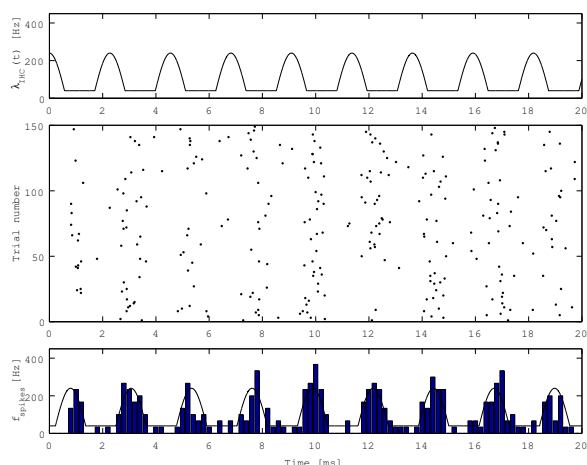


Fig. 5. Intensity function (top trace), Raster plot (middle trace), Post-stimulus time histogram with an intensity function (bottom trace) at $\lambda_{spon} = 40s^{-1}$, $\lambda_c=200 s^{-1}$, and $f = 440Hz$

When the spontaneous rate, λ_{spon} , was set at $40 s^{-1}$, the raster plot showed that the sinusoids at a frequency of 440

Hz can be better encoded into the spike trains, i.e., a greater synchronization, because the PSTH was agreed well with the intensity function, as shown in Figure 5 ($\lambda_c=200 s^{-1}$, and $f = 440Hz$).

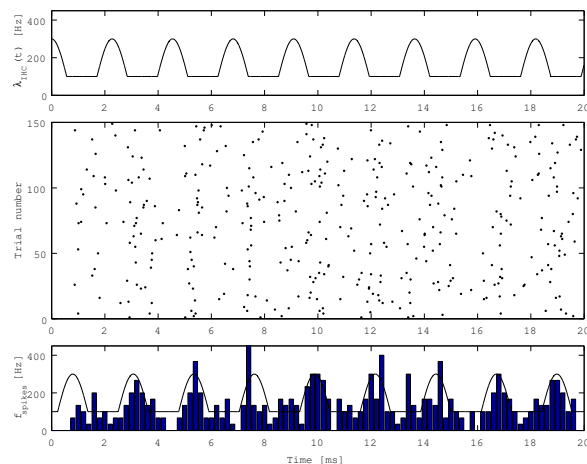


Fig. 6. Intensity function (top trace), Raster plot (middle trace), Post-stimulus time histogram with an intensity function (bottom trace) at $\lambda_{spon} = 100s^{-1}$, $\lambda_c=200 s^{-1}$, and $f = 440Hz$

As the spontaneous rate, λ_{spon} , was increased, the number of spontaneous spikes tended to increase, as shown in the raster plot of Figure 6 at $\lambda_{spon} = 100s^{-1}$, $\lambda_c=200 s^{-1}$, and $f = 440Hz$. This figure showed that the unwanted spike firings other than those modulated by the sinusoids of $440 Hz$ were observed, implying that a much greater value of λ_{spon} would make it difficult to encode accurately the sinusoidal information into the spike trains.

Although the raster plot and PSTH could give us an insight into a dependency of the spontaneous rates on sinusoidal encoding, they would only provide us with a qualitative impression. Instead, we adopted to evaluate quantitatively the information rates of the spike trains in response to the IHC synaptic currents, modulated by sinusoidal functions.

The information rates were estimated by multiplying the mutual information to the spike firing rates according to (6) in which the mutual information was estimated from observations of the ISI histograms, as the spontaneous rates, λ_{spon} , were varied to 10, 20, 30, 40, 60, 80, and $100 s^{-1}$. Figures 7-9 show the ISI histograms used in estimating the total entropy, when the spontaneous rate, λ_{spon} , was set at 10, 40, and $100 s^{-1}$.

The information rates as a function of the spontaneous rate λ_{spon} were depicted in Figure 10. The information rate was increased, maximized, and then decreased as the spontaneous rate was increased, like a typical curve of the regular stochastic resonance. This result implies a resonance phenomenon dependent on the spontaneous rate.

IV. CONCLUDING REMARKS

In this article we have observed a resonance phenomenon of spontaneous rates in an auditory nerve fiber model, stimulated by an IHC synaptic current through computer

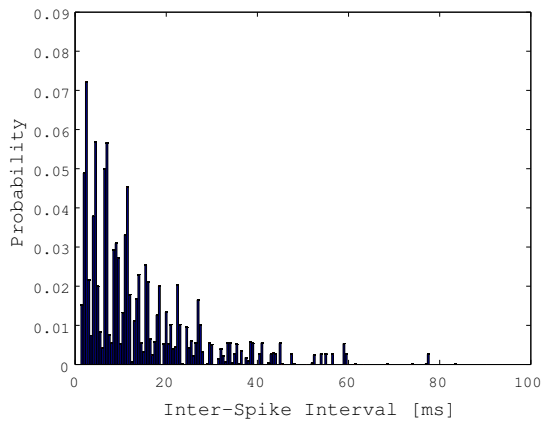


Fig. 7. Inter-Spike Interval histogram at $\lambda_{spon} = 10s^{-1}$, $\lambda_c=200 s^{-1}$, and $f = 440Hz$

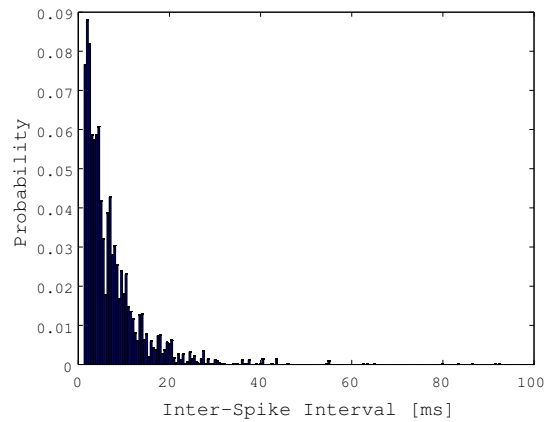


Fig. 9. Inter-Spike Interval histogram at $\lambda_{spon} = 100s^{-1}$, $\lambda_c=200 s^{-1}$, and $f = 440Hz$

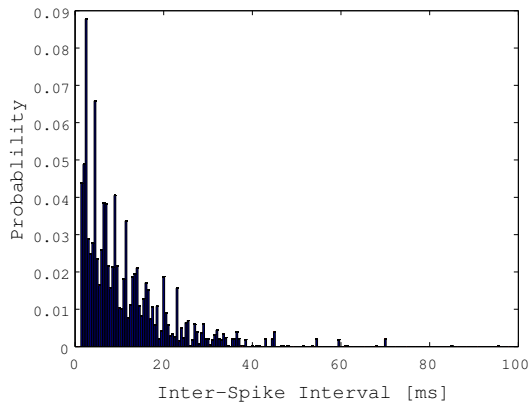


Fig. 8. Inter-Spike Interval histogram at $\lambda_{spon} = 40s^{-1}$, $\lambda_c=200 s^{-1}$, and $f = 440Hz$

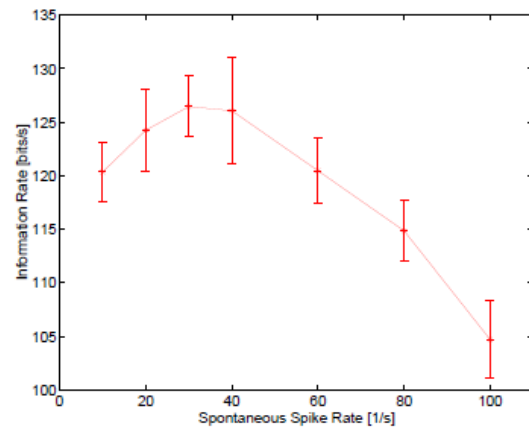


Fig. 10. The relation between the spontaneous rate of the IHC synaptic vesicle secretions and the information rate of the spike trains in the ANF model

simulations. The results show that the information rate can be maximized at a specific rate of the spontaneous spikes at about $40 s^{-1}$, consistent with those reported in animal experiments of cats [2], [3]. However, we could not cite the relationship between the spontaneous spike rates and the functional role in relaying information on the sound stimuli into sub-divisions of the cochlear nucleus in the brainstem. Understanding the functional role of the spontaneous spikes in auditory nervous systems will be given to an opportunity in the future. These findings may advance our understanding of information transmission in auditory nerves and may accelerate the design of better auditory prostheses.

REFERENCES

[1] D. L. Snyder and M. I. Miller, *Random Point Processes in Time and Space*, Second Edition, Springer-Verlag, New York, 1991.
 [2] L. C. Liberman, "Auditory-nerve response from cats raised in a low-noise chamber," *J. Acoust. Soc. Am.*, 63, pp.442-455, 1978.
 [3] L. C. Liberman, "Single-neuron labeling in the cat auditory nerve," *Science*, 216, pp.1239-1241, 1982.

[4] L. C. Liberman, "Central projections of auditory-nerve fibers of different spontaneous rate I. Anteroventral cochlear nucleus," *J. Comp Neurol.*, 313, pp.240-258, 1991.
 [5] L. C. Liberman, "Central projections of auditory-nerve fibers of different spontaneous rate II. Posteroventral and dorsal cochlear nuclei," *J. Comp Neurol.*, 327, pp.17-36, 1993.
 [6] J. T. Rubinstein, B. S. Wilson, C. C. Finley, and P.J. Abbas, "Pseudospontaneous activity : stochastic independence of auditory nerve fibers with electrical stimulation," *Hear. Res.*, 127, pp.108-118, 1999.
 [7] H. Mino, J.T. Rubinstein, and C. A. Miller, and P.J.Abbas, "Effects of Electrode-to-Fiber Distance on Temporal Neural Response with Electrical Stimulation," *IEEE Trans. on Biomed. Eng.*, Vol.51, pp.13-20, 2004.
 [8] L.A.Cartee, "Spiral ganglion cell site of excitation ii :Numerical model analysis," *Hear. Res.*, 215, pp.22-30, 2006.
 [9] H. Mino, J.T. Rubinstein, and J. A. White, "Comparison of Computational Algorithms for the Simulation of Action Potentials with Stochastic Sodium Channels," *Ann. Biomed. Eng.*, 30, pp.578-587, 2002.
 [10] H. Mino, "Encoding of Information Into Neural Spike Trains in an Auditory Nerve Fiber Model With Electric Stimuli in the Presence of a Pseudospontaneous Activity," *IEEE Trans. on Biomed. Eng.*, Vol.54, pp.360-369 ,2007.